Structure, magnetic susceptibility, and specific heat of the spin-orbital-liquid candidate FeSc$_2$S$_4$: Influence of Fe off-stoichiometry

V. Tsurkan,[1,2,*] L. Prodan,[1] V. Felea,[1] I. Filippova,[1] V. Kravtsov,[1] A. Günther,[2] S. Widmann,[2]
H.-A. Krug von Nidda,[2] J. Deisenhofer,[2] and A. Loidl[2]

[1]*Institute of Applied Physics, Academy of Sciences of Moldova, MD-2028 Chisinau, Republic of Moldova*
[2]*Experimental Physics V, Center for Electronic Correlations and Magnetism, University of Augsburg, 86135 Augsburg, Germany*

We report structure, susceptibility, and specific heat studies of stoichiometric and off-stoichiometric poly- and single crystals of the A-site spinel compound FeSc$_2$S$_4$. In stoichiometric samples, no long-range magnetic order is found down to 1.8 K. The magnetic susceptibility of these samples is field independent in the temperature range 10–400 K and does not show irreversible effects at low temperatures. In contrast, the magnetic susceptibility of samples with iron excess shows substantial field dependence at high temperatures and manifests a pronounced magnetic irreversibility at low temperatures with a difference between zero-field cooled (ZFC) and field cooled (FC) susceptibilities and a maximum at 10 K, reminiscent of a magnetic transition. Single-crystal x-ray diffraction of the stoichiometric samples revealed a single phase spinel structure without site inversion. In single crystalline samples with Fe excess, in addition to the main spinel phase, a second ordered single-crystal phase was detected with the diffraction pattern of a vacancy-ordered superstructure of iron sulfide, close to the 5C polytype Fe$_9$S$_{10}$. Specific heat studies reveal a broad anomaly, which evolves below 20 K in both stoichiometric and off-stoichiometric crystals. We show that the low-temperature specific heat can be well described by considering the low-lying spin-orbital electronic levels of Fe^{2+} ions. Our results demonstrate significant influence of excess Fe ions on intrinsic magnetic behavior of FeSc$_2$S$_4$ and provide support for the spin-orbital liquid scenario proposed in earlier studies for the stoichiometric compound.

I. INTRODUCTION

In search for quantum states of matter, frustrated magnetic AB_2X_4 spinels have been intensively studied during the last decades. Structural complexity of the spinel lattice with two different cationic sites, in combination with inherent geometrical frustration of the pyrochlore B-site sublattice [1] and bond frustration of the bipartite diamond-type A-site sublattice [2] create a fertile ground for their unconventional and exotic behavior. Among the ternary spinels, FeSc$_2$S$_4$ holds a special place, being so far a prime candidate to manifest spin-orbital liquid (SOL) behavior, an exotic quantum state with entangled spin and orbital degrees of freedom. First magnetic studies of FeSc$_2$S$_4$ did not find magnetic ordering down to 4.2 K [3]. Further magnetic and specific-heat studies—extended down to 50 mK—did not reveal any long-range magnetic order either [4]. At the same time, the magnetic susceptibility of FeSc$_2$S$_4$ was found to follow a Curie-Weiss (CW) behavior in a very broad temperature range from 400 K down to 20 K with a high value of the CW temperature $\theta_{CW} \approx -45$ K [3,4], indicating the dominance of antiferromagnetic exchange. The frustration parameter, i.e., the ratio of the CW temperature to the ordering temperature for this compound is above 900, being one of the highest values reported so far for frustrated magnets. The lack of long-range magnetic order together with the absence of Jahn-Teller (JT) ordering at low temperatures anticipated for the orbitally degenerate tetrahedral Fe^{2+} ions allowed the authors of Ref. [4] to assign the ground state of this compound to a spin-orbital liquid. Neutron scattering studies of FeSc$_2$S$_4$ in zero field [5] confirmed the absence of long-range magnetic and of static JT order, revealing strongly

dispersive spin excitations with an excitation gap of the order of 0.2 meV. The absence of long-range magnetic order in FeSc$_2$S$_4$ was also proved by a muon spin rotation [6]. Nuclear magnetic resonance (NMR) studies of FeSc$_2$S$_4$ [7,8] have noted deviations from the CW behavior at low temperatures and a levelling off of the local magnetic susceptibility below 10 K, reminiscent of strongly frustrated spin systems. Terahertz (THz) and far-infrared investigations in zero field of the low-lying excitations in FeSc$_2$S$_4$ provided experimental evidence for the existence of a spin-orbiton excitation related to entangled spin and orbital degrees of freedom [9]. Subsequent THz spectroscopy studies under applied magnetic fields evidenced a threefold splitting of this excitation, which was attributed to a singlet-triplet transition from the SOL ground state [10]. Recent inelastic neutron-scattering measurements of FeSc$_2$S$_4$ under applied magnetic fields revealed the shift of the low-energy spectral weight to high energies upon increasing field, which was explained by the entangled spin-orbital character of the magnetic states [11]. Theoretical studies of the SOL states [12,13] predicted FeSc$_2$S$_4$ to lie near a quantum-critical point that separates the spin-orbital singlet and the spin and orbitally ordered state. In contrast to the abovementioned experimental studies, recent neutron-scattering experiments [14] found a long-range antiferromagnetic order with very small magnetic moment below 10 K and an orbitally ordered state below 80 K, thus questioning the magnetic behavior of FeSc$_2$S$_4$ reported earlier in Refs. [4–10]. The composition of samples studied in Ref. [14] was refined with 6% of Fe on the octahedral sites. These samples showed a significant temperature-independent susceptibility which was attributed to ferromagneticlike impurities, presumably due to iron sulfide phase, as reported by subsequent study on single crystals grown by floating zone method [15]. In earlier measurements [4,7], however, no noticeable temperature-independent susceptibility in FeSc$_2$S$_4$

---

*Corresponding author: vladimir.tsurkan@physik.uni-augsburg.de

was found. At the same time, in previous [4,7] and recent [11,14,15] studies of $FeSc_2S_4$, a level below 3% for site intermixing of Fe and Sc ions between the tetrahedral and octahedral sites of the spinel lattice was reported. Within such a low level of inversion, it is quite difficult to understand the contrasting magnetic behavior of samples reported in Refs. [4,7,14,15].

Here, we present structural, magnetic, and specific-heat studies of $FeSc_2S_4$ performed on poly- and single crystals with different deviations from the ideal stoichiometry. This paper evidences a detrimental effect of the excess Fe ions on intrinsic magnetic properties of $FeSc_2S_4$. We confirm the absence of the long-range magnetic order in stoichiometric $FeSc_2S_4$ and support previous conclusions concerning its spin-orbital liquid ground state.

II. EXPERIMENTAL

Polycrystalline $FeSc_2S_4$ was prepared by solid-state synthesis from high-purity elements. The off-stoichiometric samples were prepared from binary FeS and Sc_2S_3 preliminarily synthesized from the elements. The low level of inversion reported in all previous studies of $FeSc_2S_4$ indicates that Sc ions hardly penetrate into the tetrahedral A sites. This corroborates with the results of structural investigations of related off-stoichiometric spinel compounds $Fe_{0.85}Sc_{2.1}S_4$ [16] and $Mn_{2.29}Sc_{1.14}S_4$ [17], which did not reveal Sc ions at the tetrahedral A sites, but we found substantial amount of Fe on the octahedral B sites. Therefore, in the preparation of the off-stoichiometric samples, we assumed the formation of compositions $Fe_{1+x}Sc_{2-x}S_4$, in which the excess Fe ions will occupy the octahedral B sites.

The single crystals have been grown by chemical transport reactions using iodine as transport agent. The growth experiments were performed at temperatures between 900 and 950 °C for a period up to 12 weeks for each growth run.

Technical details for synthesis and single-crystal growth are given in the Supplemental Material [18].

The chemical composition of the samples was determined with an electron-probe microanalyzer CAMECA SX 50 by wavelength dispersive x-ray spectroscopy (WDS). The errors in determination of the absolute concentrations of the elements were below 1.5% for Fe and 2% for Sc and S.

The single-crystal x-ray diffraction was performed at room temperature with a Xcalibur E diffractometer equipped with a charge-coupled device (CCD) area detector and a graphite monochromator utilizing Mo Kα radiation. The analysis of diffraction pattern, the search and refinement of unit cell parameters, has been done using CrysAlisPro, Agilent Technologies program suite, version 1.171.37.35 [19]. Final unit cell dimensions were obtained and refined on an entire dataset. After collection and integration, the data were corrected for Lorentz and polarization effects and for absorption by multiscan empirical absorption correction methods. The structures were refined by the full matrix least-squares method based on F^2 with anisotropic displacement parameters. All calculations were carried out by the programs SHELXL2014 [20]. Crystallographic data and details on the structure refinement for the single crystalline samples are given in Table SM3. The x-ray diffraction of polycrystals was performed with a

conventional laboratory x-ray diffractometer (STOE Stadi P) with Cu Kα radiation. The data were analyzed with a standard Rietveld refinement using the FULLPROF Suite program [21].

Magnetic characterization was performed using a commercial SQUID magnetometer (MPMS-5, Quantum Design) for temperatures between 1.8 and 700 K and in external magnetic fields up to 5 T. The specific heat was measured with a Physical Properties Measurement System (PPMS, Quantum Design) in the temperature range from 1.8 to 300 K.

III. RESULTS AND DISCUSSION

A. Compositional analysis

In Table I, the results of the WDS analysis of the composition of several poly- and single crystalline samples are given. Within the accuracy of the analysis, the composition of the polycrystalline samples, prepared from the stoichiometric ratio of the elements, was close to that for the ideal stoichiometry (see Table S1 of the Supplemental Material [18]). Similar results were found for single crystalline samples, although a deficiency of iron, varying between 2 and 5 at.%, was observed in different samples from the same batch. An excess of Fe of ~23 at.% and a respective deficiency of ~23 at.% for Sc compared to ideal stoichiometry was revealed in the off-stoichiometric single crystals. Similar results were found for polycrystalline samples with Fe excess. These data appear to be in reasonable agreement with the formation of compositions $Fe_{1+x}Sc_{2-x}S_4$ with the excess Fe ions on the octahedral sites. Surprisingly, single-crystal x-ray studies of these samples (presented below) contradict this intuitive assumption.

B. X-ray diffraction

In Figs. 1(a) and 1(b), the x-ray diffraction patterns are presented for single crystals with ideal stoichiometry composition ($x = 0$) and off-stoichiometric composition (with iron excess $x = 0.23$), respectively. The diffraction pattern for the stoichiometric sample corresponds to a single phase consistent with the spinel structure of $Fd\bar{3}m$ symmetry (#227). In contrast, the diffraction pattern for the sample with off-stoichiometric composition $x = 0.23$ reveals two clearly distinct phases. The analysis of diffraction pattern shows that 1558 of the total 1721 observed diffraction reflections correspond to a spinel phase (about 90.7%), shown in Fig. S2(a) of the Supplemental Material [18], and 159 (about 9.3%) to a minority phase, the reflections of which also form an ordered pattern shown in Fig. S2(b) of the Supplemental Material [18]. The second phase has been indexed in a cubic system with a rather high value of the lattice constant of 14.82 Å. In fact, for the essentially longer exposure time of data collection, the reflections of smaller intensity became visible, and regular patterns with even higher lattice constant $a \approx 29.74$ Å were observed. Such a regular pattern of the minority phase reminds one of the ordered-vacancy structure characteristics of many binary iron sulfides and selenides. Our magnetic study of samples with Fe excess presented in the following section reveals a ferromagneticlike contribution of the impurity phase at high temperatures, which we primarily associate with a ferrimagnetic NiAs-type Fe_7S_8 phase by

TABLE I. Composition of $Fe_{1+x}Sc_{2-x}S_4$ samples determined by WDS analysis.

Sample	Fe (Wt.%)	Sc (Wt.%)	S (Wt.%)	Sum (Wt.%)	Composition
Ideal stoichiometry $x = 0$	20.38	32.81	46.81	100.00	$FeSc_2S_4$
ATF526 $x = 0$, poly	20.65(47)[a]	33.27(55)	46.90(50)	100.82(83)	$Fe_{1.006(19)}Sc_{2.000(33)}S_{3.977(29)}$
ATR236M1 $x = -0.02$, mono	20.25(15)	32.48(34)	46.18(17)	98.91(36)	$Fe_{1.003(10)}Sc_{2.000(14)}S_{3.991(10)}$
ATR236M5 $x = 0$, mono	20.24(22)	32.42(43)	46.03(31)	98.69(62)	$Fe_{0.992(12)}Sc_{2.000(21)}S_{3.928(19)}$
ATR215M2 $x = -0.02$, mono	20.04 (19)	33.22(21)	46.55(26)	99.81(56)	$Fe_{0.980(8)}Sc_{2.020(13)}S_{3.974(11)}$
ATR215M3 $x = -0.05$, mono	19.50(13)	32.98(28)	46.71(20)	99.19(43)	$Fe_{0.952(6)}Sc_{2.000(14)}S_{3.965(16)}$
ATF522 $x = 0.06$, poly	22.06(16)	31.88(12)	45.75(29)	99.69(38)	$Fe_{1.073(7)}Sc_{1.927(10)}S_{3.881(12)}$[b] $0.972FeSc_2S_4 + 0.122Fe_{0.9}S$
ATF527 $x = 0.12$, poly	22.37(20)	31.33(34)	46.43(45)	100.13(38)	$Fe_{1.098(9)}Sc_{1.910(19)}S_{3.959(16)}$[b] $0.955FeSc_2S_4 + 0.158Fe_{0.9}S$
ATF540 $x = 0.24$, poly	24.26(31)	29.44(34)	45.71(44)	99.41(67)	$Fe_{1.190(15)}Sc_{1.794(20)}S_{3.906(38)}$[b] $0.897FeSc_2S_4 + 0.326Fe_{0.9}S$
ATR268M1 $x = 0.22$, mono	24.83(30)	28.94(17)	46.40(16)	100.17(31)	$Fe_{1.218(13)}Sc_{1.764(11)}S_{3.965(16)}$[b] $0.882FeSc_2S_4 + 0.362Fe_{0.9}S$
ATR268M3 $x = 0.23$, mono	25.04(23)	29.08(20)	46.45(33)	100.57(21)	$Fe_{1.229(12)}Sc_{1.773(14)}S_{3.969(17)}$[b] $0.886FeSc_2S_4 + 0.380Fe_{0.9}S$

[a]Standard deviations are given in parentheses.

[b]Calculated composition for two coexisting phases.

analogy to Ref. [15]. Nonstoichiometric $Fe_{1-\delta}S$ is known to manifest a variety of different superstructures depending on the preparation conditions and on deviation from the stoichiometry [22,23]. We noticed also that the lattice constant of the second phase in our off-stoichiometric sample is close to that of the 5C polytype of pyrrhotite Fe_9S_{10} [24].

Details of the structural refinement together with the crystal parameters for different single crystalline samples are given in Table S3 of the Supplemental Material [18]. The crystal structure of the stoichiometric samples corresponds to a normal spinel with Fe ions exclusively at $8a$ sites and Sc ions at $16d$ sites. The refinement of site occupation factors for Sc and Fe positions reveals deviations from the expected values (0.08333 and 0.04167, respectively) of less than two and about three estimated standard deviations (e.s.d.). Thus, within the accuracy of refinement, no site inversion was detected for

FIG. 1. (a) Image of experimental x-ray diffraction pattern for a stoichiometric single crystal ($x = 0$). (b) Image of experimental x-ray diffraction pattern for an off-stoichiometric single crystal with Fe excess ($x = 0.23$). Green color corresponds to b^* and c^* axes of the unit cell of the minority phase (see Fig. S2 of the Supplemental Material [18]).

these samples. Similar results were obtained for samples with Fe deficiency and Fe excess, where intensity of diffraction reflections has been obtained by integration over positions of the peaks corresponding to spinel phase. The deviation of site occupation factors for Sc and Fe positions from the expected values for the spinel phase do not exceed two e.s.d. We also noticed enhanced thermal displacement parameters for ions in samples with Fe excess compared to that for the stoichiometric samples (see Table S4 of the Supplemental Material [18]). This additional feature in samples with Fe excess can be related to the influence of the second (impurity) phase.

Figure 2 presents the x-ray powder diffraction patterns for polycrystalline samples $Fe_{1+x}Sc_{2-x}S_4$ with different x. All spectra surprisingly show only reflections characteristic of the spinel structure without noticeable impurity peaks. Only in the sample with the highest iron excess $x = 0.24$, a small peak centered at $2\theta = 43.5°$ (marked by an asterisk) becomes pronounced over the background. Its angular position correlates well with the maximal peak of the x-ray diffraction spectra for Fe_7S_8 shown at the bottom of Fig. 2. On increasing x, broadening of the reflections (shown in the inset of Fig. 2) and progressive growth of the background level take place.

Like in polycrystals, stoichiometric single crystalline samples and samples with slight iron deficiency ($x = -0.02$) show diffraction patterns with much narrower lines compared to samples with iron excess $x = 0.23$ (see Fig. S3 of the Supplemental Material [18]). In the later off-stoichiometric sample also, only a single impurity peak of small intensity was detected like in the polycrystalline sample with $x = 0.24$, although the single-crystal x-ray diffraction documented a significant amount (of ~9%) of the second phase.

The Rietveld refinement of the x-ray powder diffraction patterns for samples was done assuming several structural models: (a) normal spinel with Fe ions only at $8a$ sites and Sc ions at $16d$ sites; (b) inversion model with intermixing of Fe
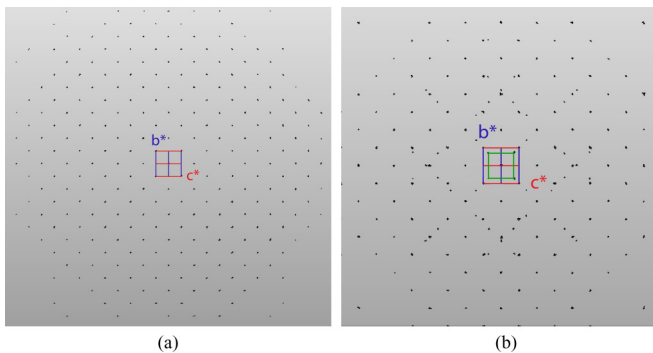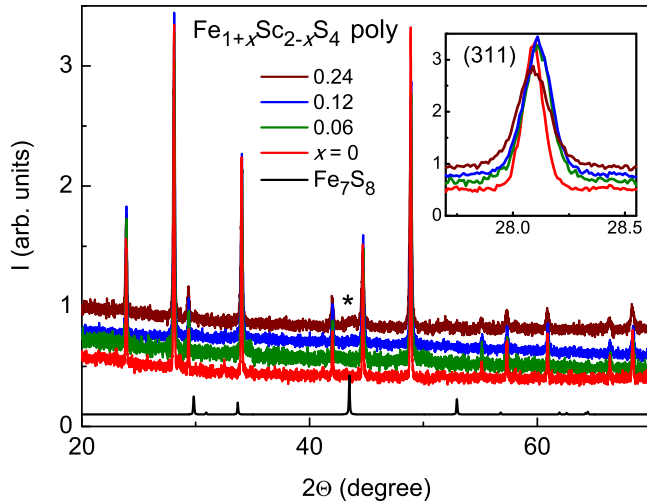
FIG. 2. X-ray diffraction patterns for polycrystalline samples $Fe_{1+x}Sc_{2-x}S_4$ with different x and of Fe_7S_8 (black bottom line). The asterisk marks the impurity peak in sample with $x = 0.24$. The inset shows the (311) reflections on enlarged scale demonstrating broadening of the reflections and increasing background in samples with increasing x.

and Sc between $8a$ and $16d$ sites; (c) Fe distributed between $8a$, $16d$, and $16c$ sites, and Sc between $16d$ and $16c$ sites proposed previously in Refs. [16,17]; (d) two-phase model with a main spinel phase of stoichiometric composition and an impurity phase of iron sulfide. The details and results of the refinement are given in the Supplemental Material [18].

Within the inversion model for refinement of the diffraction pattern for polycrystalline samples and powdered single crystalline samples, an intermixing of cations between the A and B sites up to a level to 3% was obtained. A similar low level of inversion of 2.8(8)% in one of the stoichiometric polycrystalline samples (ATF 526) was established by recent high-resolution x-ray and neutron-powder diffraction studies performed in Ref. [11]. However, taking into consideration the results of the single-crystal diffraction of the stoichiometric samples, we think that the calculated level of inversion characterizes rather the accuracy of refinement of the powder pattern than the real inversion which appears to be negligible.

The refinement for samples with Fe excess did not reveal Fe ions at $16c$ sites of the spinel lattice. Within the inversion model, a level up to 4% of Fe at $16d$ sites was obtained. No respective amount of Sc ions at the A sites was found.

The lattice parameters of the spinel phase for samples with different x (given in the Table S5 of the Supplemental Material [18]) show only small variation, which can probably be attributed to details of the sample preparation, e.g., minor deviations from the stoichiometry, difference in regimes of thermal treatments, treatment atmosphere, etc. Importantly, rather low scattering of values of the lattice constants for samples with different x indicates high structural stability of the main spinel phase and suggests an insignificant level of inversion.

Summarizing the results of the structural analysis, we can fully exclude the inversion for stoichiometric $FeSc_2S_4$ samples. The x-ray diffraction analysis points also to a small inversion degree (probably also absent) in the main spinel

phase in samples with Fe excess. The excess Fe ions form a second phase of iron sulfide which intergrows with the main spinel phase.

Thus, our results indicate that, from the powder diffraction pattern only, it is rather difficult to conclude about the phase content and purity of the samples. The absence of visible impurity reflections in powder diffraction spectra of the off-stoichiometric samples containing a substantial amount of impurity phase (revealed by susceptibility and single-crystal x-ray studies) can explain the apparently contradictory results reported in Refs. [14,15] and our results concerning the stoichiometry and phase content of the studied samples.

Based on the results of the structural analysis of the off-stoichiometric samples, which provide evidence for coexistence of the main stoichiometric spinel phase and the second phase of iron sulfide, we reanalyzed the data of the WDS compositional analysis, which are also presented in Table I. We got a reasonable agreement concerning the amount of the main and the second phase in the off-stoichiometric single crystalline samples with those obtained from the single-crystal diffraction. Within the accuracy of the WDS analysis, the composition of the off-stoichiometric polycrystalline samples can be well described by a two-phase model with decreasing concentration of the main phase as $(1 - x/2)FeSc_2S_4$ and increasing concentration of the second phase as $(3x/1.8)Fe_{0.9}S$ on increasing of Fe excess x.

C. Magnetic properties

The temperature dependences of the magnetic susceptibility χ and of the inverse susceptibility for several stoichiometric $FeSc_2S_4$ poly- and single crystals ($x = 0$) measured in a field of 1 T are shown in Fig. 3. In agreement with previous studies [3,4], for stoichiometric samples, we observed an extended temperature range (from 10 to 400 K) of CW behavior of the susceptibility with very similar values of χ for samples from different batches. The susceptibility for these poly- and single crystals amounts to $\sim 7.5 * 10^{-3}$ emu/mol at 400 K. For stoichiometric samples, no significant temperature-independent susceptibility is revealed. Its amount is estimated at a level of $\sim 0.3 * 10^{-3}$ emu/mol. These samples contain only a single spinel phase, and therefore, we can attribute the measured susceptibility to an intrinsic susceptibility of stoichiometric $FeSc_2S_4$. Below 6 K, the susceptibility of the stoichiometric polycrystalline sample shows a slight upturn, which reminds one of a Curie tail due to possible residual magnetic impurities. However, a similar upturn in χ at low temperatures was observed in our stoichiometric single crystals, where the amount of residual magnetic impurities is anticipated at a much lower level than in polycrystals. Note that the susceptibilities of our stoichiometric samples reveal pronounced field dependence only at temperatures below 6 K, as shown in the inset of Fig. 3. The susceptibility levels off at high fields and at lowest temperatures. At the same time, at temperatures above 6 K, the susceptibility of stoichiometric samples is found to be completely field independent. In the case of impurities originating from the ferrimagnetic $Fe_{1-\delta}S$ with a Curie temperature of 588 K [25], the susceptibility is expected to be clearly field dependent at high temperatures, where the contribution from the intrinsic
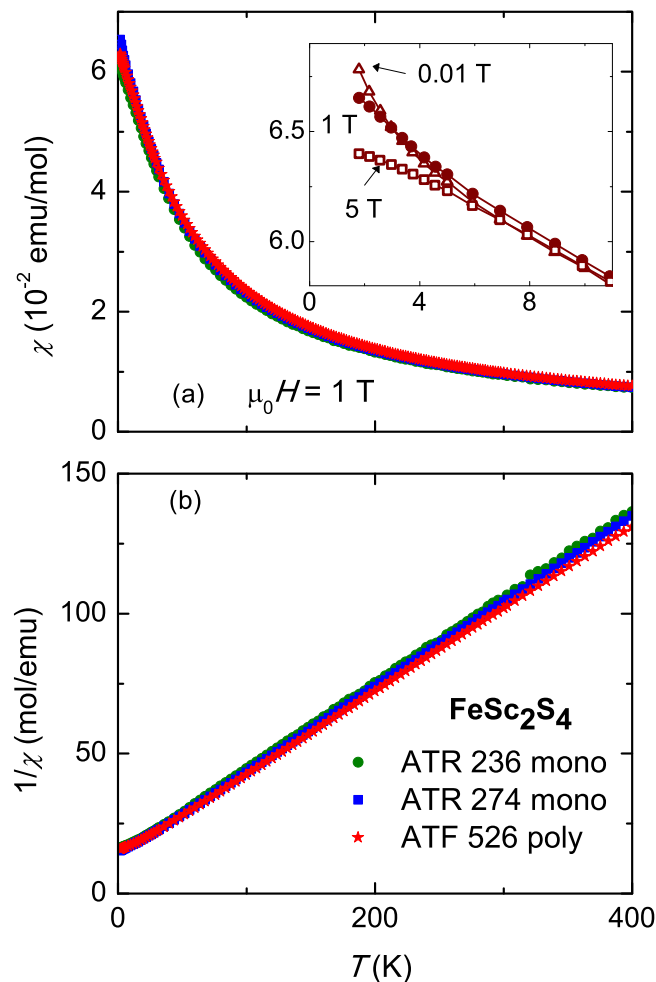
FIG. 3. Temperature dependences of (a) the magnetic susceptibility and (b) the inverse susceptibility, measured in a magnetic field of 1 T for stoichiometric polycrystalline and single crystalline samples of $FeSc_2S_4$. Inset in (a) shows the susceptibility of the stoichiometric single crystal measured at different applied magnetic fields for the temperature range below 10 K.
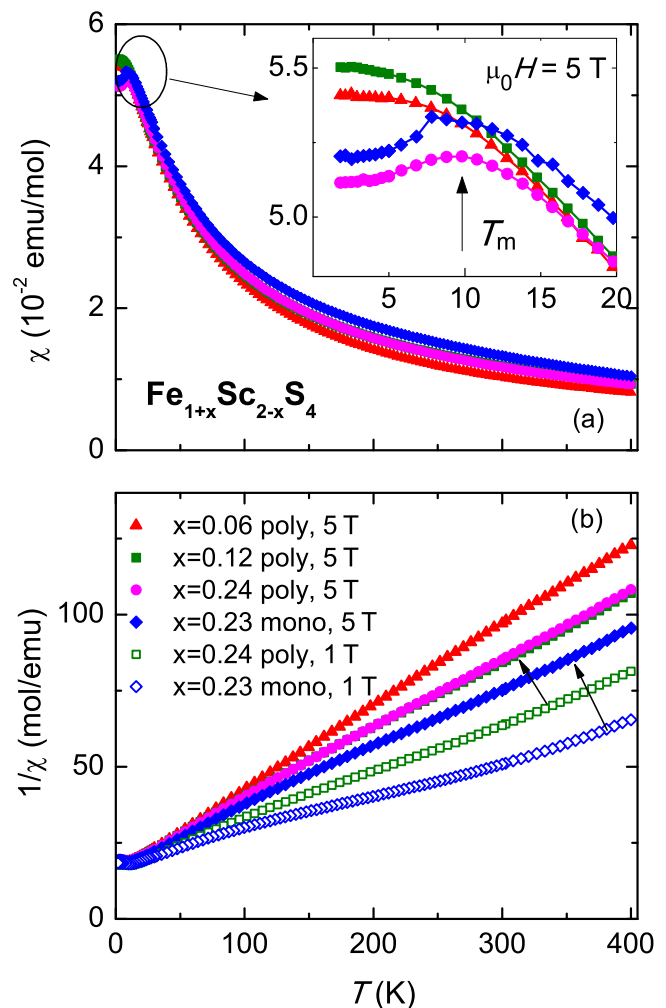
FIG. 4. Temperature dependences of (a) the magnetic susceptibility and (b) the inverse susceptibility, measured in magnetic fields of 5 T (closed symbols) and 1 T (open symbols) for poly- and single crystalline samples with iron excess. Inset in (a) shows the susceptibility behavior below 20 K on an enlarged scale. The vertical arrow marks the maximum in the susceptibility at $T_m \approx 10$ K. The arrows in (b) show the shift of the $\chi^{-1}(T)$ dependences on increasing field from 1 to 5 T, demonstrating strong field dependence of the susceptibility of the samples with Fe excess.

susceptibility of the spinel phase $FeSc_2S_4$ is strongly reduced. Such a field-dependent behavior of the susceptibility at high temperatures, however, was not observed in our stoichiometric samples. Therefore, we conclude that the susceptibility upturn observed in stoichiometric samples at low temperatures and in low fields is not related to $Fe_{1-\delta}S$ impurities. The levelling off of the local susceptibility at temperatures below 10 K detected in NMR studies of $FeSc_2S_4$ [6,7] correlates well with our susceptibility data for an applied field of 5 T and thus cannot be related to impurities either.

In contrast to stoichiometric samples, the susceptibility of samples with iron excess was found to be strongly field dependent in the temperature range 10–400 K. Figure 4(a) shows the temperature dependences of the magnetic susceptibilities and Fig. 4(b) of the inverse susceptibilities for poly- and single crystals with iron excess measured in a field of 5 T. The application of a higher field was necessary to saturate impurity contribution to the magnetization of these samples, which will be further discussed below. The significant difference in values

of the susceptibility χ for fields of 1 and 5 T is demonstrated in Fig. 4(b). Note also that the temperature dependence of the inverse susceptibility in a field of 1 T is highly nonlinear compared to the strictly linear dependence observed in the stoichiometric samples [Fig. 3(b)]. Below 20 K, the susceptibility for polycrystalline samples with Fe excess $x = 0.06$ and 0.12 shows a hump at around 10 K and levels off at lower temperatures at values notably smaller than for stoichiometric samples [see insets in Figs. 3(a) and 4(a)]. In poly- and single crystalline samples with higher iron excess $x = 0.24$, the susceptibility develops a well-pronounced maximum at 10 K, reminiscent of a magnetic transition (see Fig. S5 of the Supplemental Material [18]). The other important observation is that the values of the susceptibilities of samples with iron excess at high temperatures are significantly higher compared

to stoichiometric ones (see Table S6 of the Supplemental Material [18]). Above 100 K, the susceptibility of the off-stoichiometric sample (with $x = 0.24$) for the field of 5 T shows an almost temperature-independent contribution (see Fig. S6 of the Supplemental Material [18]). We note that the values of the susceptibilities of the off-stoichiometric samples at high temperatures are similar to those documented in Refs. [14,15]. There, a temperature-independent contribution χ_0 varying from 3.1×10^{-2} emu/mol for polycrystalline samples to 1.77×10^{-1} emu/mol for single crystals was reported, values which are 4 to 23 times higher than the intrinsic susceptibilities of our stoichiometric samples at temperatures above 100 K. Taking into consideration a ferromagneticlike behavior of the susceptibility under magnetic field observed in our poly- and single crystalline samples with iron excess, we attribute it to the second phase revealed by single-crystal diffraction.

To clarify the origin of the second magnetic phase existing in samples with Fe excess, we extended the susceptibility measurements to temperatures up to 700 K. In Fig. 5, we present, respectively, the temperature dependences of (a) the magnetic susceptibility and (b) inverse susceptibility measured in a magnetic field of 0.1 T for polycrystalline sample with Fe excess $x = 0.24$ at temperatures between 300 and 700 K. The data measured on heating document a clear magnetic phase transition at $T_C = 580$ K with a thermal hysteresis of ~ 20 K on cooling cycle. Above T_C, the susceptibility of this sample follows a CW law indicating a true paramagnetic state. Note that very similar magnetic behavior was reported in Ref. [25] for ferrimagnetic iron sulfide $Fe_{0.902}S$. These results suggest that the second magnetic phase detected in our off-stoichiometric samples can be associated with the phase $Fe_{1-\delta}S$ with $\delta \approx 0.098$, i.e. a composition close to the 5C pyrrhotite Fe_9S_{10}.

The magnetic parameters, specifically the effective magnetic moment p_{eff} and the CW temperature Θ_{CW}, determined from the CW fits to the experimental data are summarized in Table S6 of the Supplemental Material [18]. For stoichiometric samples, Θ_{CW} and p_{eff} were calculated for the temperature range $20-400$ K, where a strict linear temperature dependence of the inverse susceptibility measured in a field of 1 T was observed. The values of these parameters scatter in a narrow range around -45 K and $5.15\mu_B$, respectively. The latter is in good agreement with the single-ion value for Fe^{2+} ions with a g factor of 2.07 [26]. The effective magnetic moment and the CW temperature for samples with off-stoichiometric iron were calculated from the data measured in a field of 5 T to reduce the field-dependent effects. The values of p_{eff} and Θ_{CW} are found to be increased compared to those for the stoichiometric samples. Similar enhanced values of Θ_{CW} and p_{eff} were reported for crystals studied in Ref. [15]. However, in our opinion, the values of p_{eff} and Θ_{CW} for the off-stoichiometric samples have to be considered with caution since our experiments show that the true paramagnetic state in these samples is reached only above 580 K.

To understand the reason for the different magnetic behavior of samples with stoichiometric and off-stoichiometric composition, we focused on their low-temperature magnetic properties. We found that poly- and single crystalline samples of stoichiometric $FeSc_2S_4$ exhibit a linear increase of
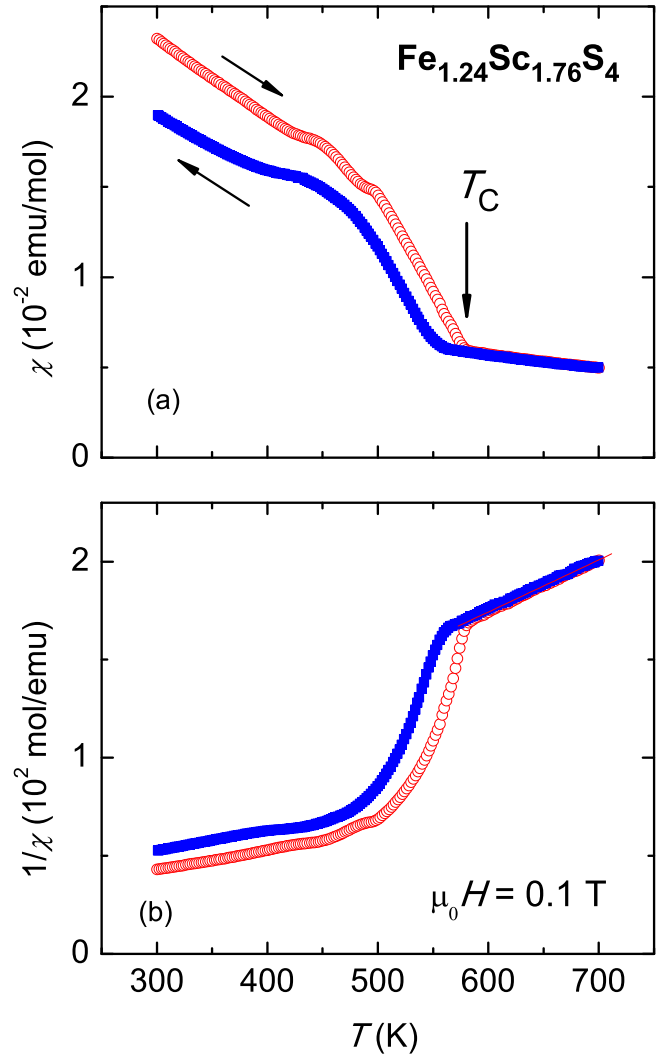

FIG. 5. Temperature dependences of (a) the magnetic susceptibility and (b) the inverse susceptibility, measured in a magnetic field of 0.1 T for the polycrystalline sample with Fe excess $x = 0.24$. Vertical arrow marks the magnetic transition on heating cycle.

the magnetization with field and no hysteretic effects (see Fig. S7 of the Supplemental Material [18]). In contrast, samples with iron excess show a significant hysteresis of magnetization with the appearance of remnant magnetization and coercive field, which both increase with increasing iron excess, as documented in the inset of Fig. S7 of the Supplemental Material [18]. The hysteresis loop closes in fields above 3 T, which is comparable with the saturation field of the ferrimagnetic phase of iron sulfide. The temperature dependence of the remnant magnetization M_r measured on the sample with the highest $x = 0.24$ reveals a sharp decrease of M_r at 10 K and a hump at around 20 K followed by a continuous decrease at high temperatures (see Fig. S8 of the Supplemental Material [18]). Even at 400 K, M_r has a nonzero value vanishing at higher temperatures, probably at T_C.

The measurements of the dc susceptibility in the low-field range using conventional zero-field cooled (ZFC) and field cooled (FC) sequences evidenced a clear contrast in the behavior of stoichiometric and off-stoichiometric samples
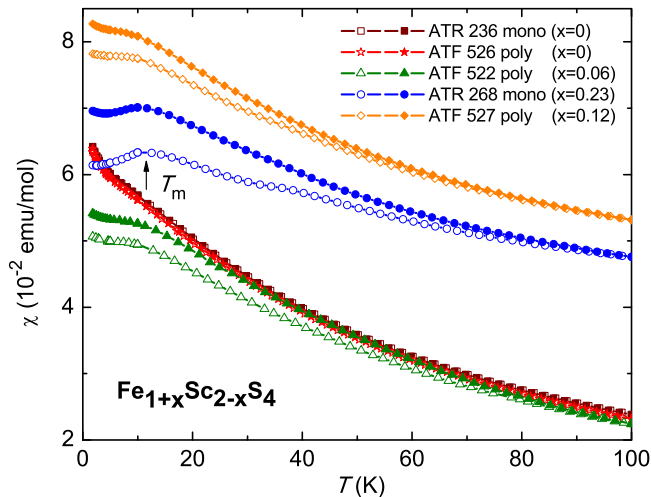
FIG. 6. Temperature dependences of the dc susceptibilities measured in a magnetic field of 0.01 T for poly- and single crystalline samples with different Fe content. Open and closed symbols mark ZFC and FC data, respectively. Vertical arrow marks the maximum at T_m.

(Fig. 6). We observed that the susceptibility for both poly- and single crystalline samples of stoichiometric $FeSc_2S_4$ exhibits only a monotonic increase with decreasing temperature. No detectable difference between ZFC and FC data was observed for stoichiometric samples that documents a negligible level of magnetic disorder. Similar behavior was found in samples with iron deficit of 5%. In contrast, strong magnetic irreversibilities were revealed for samples with Fe excess, which were reflected by a pronounced difference between ZFC and FC curves reminiscent of spin-glasslike behavior. The ZFC and FC curves split at approximately 80 K and flatten below 10 K. In the single crystal with the highest concentration of excess iron $x = 0.23$, in addition to irreversible behavior, the susceptibility develops a clear maximum at around 10 K. A similar maximum in the susceptibility at 10 K was observed in the polycrystalline sample with iron excess $x = 0.24$ (see Fig. S5 of the Supplemental Material [18]). We note that the irreversible behavior of the low-field susceptibilities observed in off-stoichiometric polycrystalline samples is again very similar to that reported for samples in Refs. [14,15]. Our results thus indicate a relation between the magnetic irreversibility effects and the second phase formed by excess Fe.

The ac susceptibility studies performed in a frequency range 1–1000 Hz also revealed different behavior for stoichiometric and off-stoichiometric samples. In the stoichiometric sample, the susceptibility was found to be frequency independent and continuously increasing with decreasing temperature, similar to dc data (Fig. 6), indicating the absence of any magnetic ordering. In contrast, susceptibility of the sample with iron excess $x = 0.23$ exhibits a nonmonotonic temperature behavior with a broad maximum centered at 11 K (see Fig. S9 of the Supplemental Material [18]). The susceptibility of this off-stoichiometric sample also is found to be frequency independent. Such a behavior of the susceptibility is in disagreement with that expected for conventional spin glasses or cluster glasses which exhibit pronounced frequency dependence [27].

In fact, the observed behavior of ac and dc susceptibilities of samples with iron excess below 20 K either suggests the onset of the antiferromagnetic order or anomalous magnetic behavior due to the second phase detected in these samples. The observation of partial antiferromagnetic spin ordering with reduced moment in Ref. [14] seems to favor the first scenario. However, in our opinion, one cannot exclude an anomalous magnetic behavior due to interaction at the interface of the main spinel phase $FeSc_2S_4$ with the secondary phase of $Fe_{1-\delta}S$ revealed in these samples. Very similar magnetic behavior as in off-stoichiometric samples was reported recently for monoclinic pyrrhotite at low temperatures due to interaction at the interface of the two coexisting superstructures 4C and $5C^*$ of $Fe_{6.6}S_8$ resulting from the change of magnetocrystalline anisotropy [28,29]. Further studies are evidently necessary to discriminate between the two possible scenarios of anomalous magnetic behavior at low temperatures observed in the off-stoichiometric samples.

D. Specific heat

In Fig. 7, the temperature dependences of the specific heat C for stoichiometric and off-stoichiometric samples measured in zero field at ambient pressure are shown. The specific heat for all samples reveals a similar continuous decrease on lowering the temperature from 300 to 20 K. No sharp anomaly or jump indicative of long-range magnetic or structural transformations at lower temperatures was found in any sample. Instead, a broad Schottky-like contribution develops at temperatures below 20 K, both for stoichiometric and nonstoichiometric samples. When plotting the specific heat as C/T vs T shown in the inset of Fig. 7, this broad anomaly is centered at 7.37, 8.23, and 8.40 K, respectively, for stoichiometric ($x = 0$), and off-stoichiometric samples with iron excess $x = 0.06$ and $x = 0.24$. The observed behavior of C for stoichiometric samples is in complete agreement with a previous report on the specific heat [4]. The behavior of C/T for our off-stoichiometric samples is similar to that reported in recent studies in Refs. [14,15].
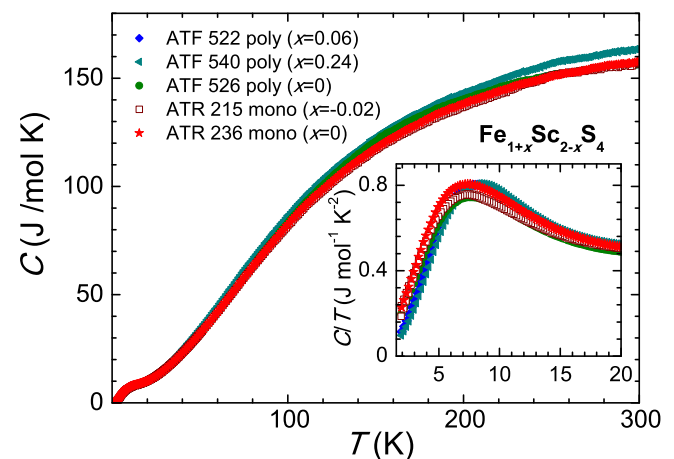

FIG. 7. Temperature dependences of the specific heat C for stoichiometric and off-stoichiometric samples. Inset presents the low-temperature data in a representation C/T on an enlarged scale, showing the shift of the maximum in C/T to higher temperatures with increasing excess of Fe.
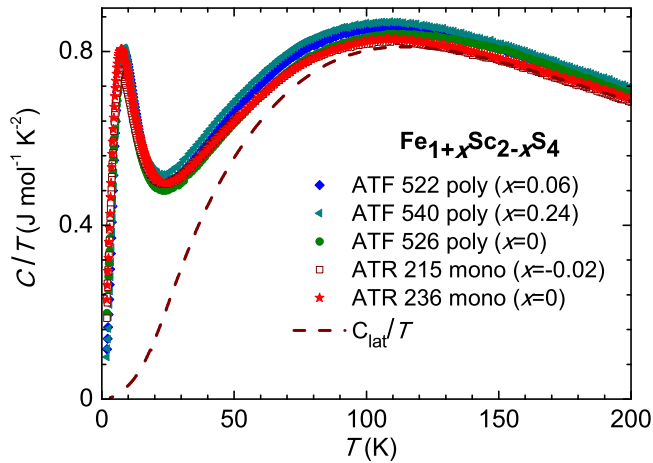
FIG. 8. Temperature dependences of the specific heat C divided by temperature T for stoichiometric and off-stoichiometric samples. The dashed line marks the lattice contribution.

Figure 8 shows the temperature dependences of the specific heat, in a representation C/T vs T at temperatures up to 200 K. At temperatures below the maximum in C/T, the specific heat of the off-stoichiometric samples is lower than that of the stoichiometric samples, while above 20 K, it shows higher values than for the stoichiometric samples. The dashed line in Fig. 8 presents the lattice contribution to the specific heat of $FeSc_2S_4$, which was calculated from the experimentally measured specific heat of the related spinel $ZnSc_2S_4$. This nonmagnetic compound differs by only 3.5% in molar mass compared to $FeSc_2S_4$. Using a combined Debye-Einstein model, we were able to describe the specific heat of the nonmagnetic $ZnSc_2S_4$ within the accuracy of $\sim 0.5\%$ in the temperature range from 40 to 250 K (see Fig. S10 of the Supplemental Material [18]). The calculated phonon contribution is found to be more accurate compared to that estimated from the specific heat data of $CdIn_2S_4$ with a much larger difference in the molar mass (by 72%) compared to $FeSc_2S_4$. The phonon contribution to the specific heat for the stoichiometric $FeSc_2S_4$ samples for temperatures above 50 K was simulated by one isotropic Debye (D) and three isotropic Einstein terms ($E1, E2,$ and $E3$). The 21 degrees of freedom per formula unit were taken into account by setting the ratio of these contributions to $D : E1 : E2 : E3 = 1 : 1 : 3 : 2$ using the Debye and Einstein temperatures $\theta_D = 183$ K, $\theta_{E1} = 175$ K, $\theta_{E2} = 340$ K, $\theta_{E3} = 497$ K, which are consistent with the frequency ranges where infrared (IR) active phonons have been observed [9].

We analyzed the experimental data by assuming two different contributions to the specific heat, namely from vibrational degrees of freedom and from the lowest-lying electronic levels of the Fe^{2+} ions. The lattice contribution C_{lat} has been subtracted from the experimentally observed specific heat. The remaining residual specific heat C_m/T for stoichiometric and off-stoichiometric samples and the entropies obtained by integrating C_m/T data are shown in Figs. 9(a) and 9(b), respectively. The entropy contained in the residual specific heat for the stoichiometric single crystalline samples saturates close to the value of $R\ln(10)$ consistent with that expected for the spin $R\ln(2S + 1)$ and orbital $R\ln2$ degrees
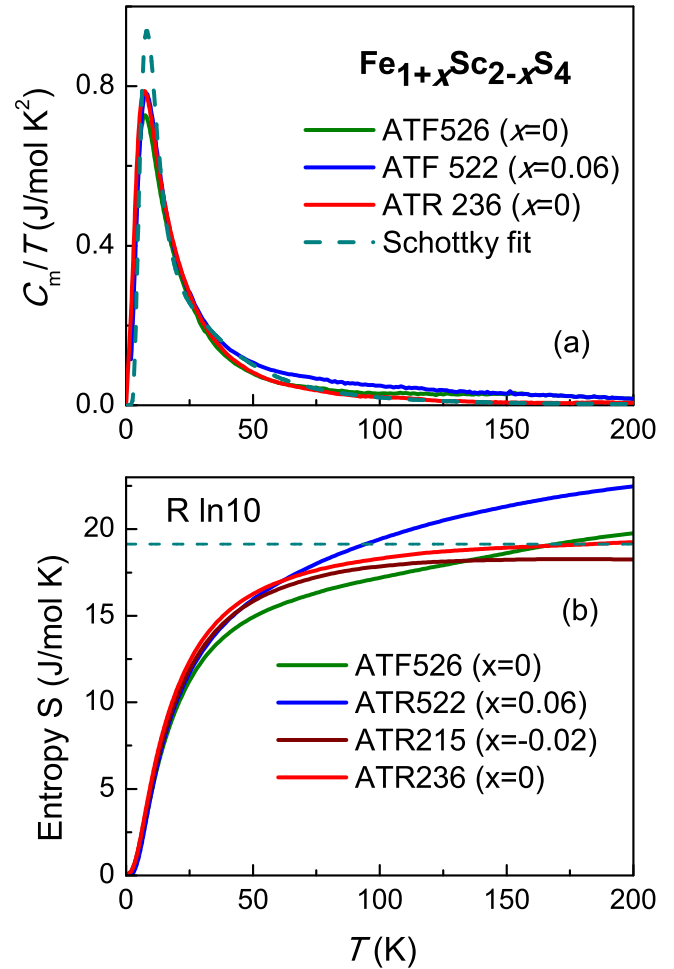

FIG. 9. Temperature dependences of the magnetic part of (a) the specific heat C_m and (b) the entropy for stoichiometric and off-stoichiometric samples. Dashed lines marks the entropy expected for the spin $R\ln(2S + 1)$ and orbital $R\ln2$ degrees of freedom.

of freedom. The deviations from the value of $R\ln(10)$ for the entropy of the nonstoichiometric samples above 100 K can probably be attributed to the second phase. Note that the estimations of the lattice contribution based on the specific heat data for heavier $CdIn_2S_4$ performed in Refs. [14,15] resulted in a significantly lower value ($\sim R\ln4$) of the entropy contained in the magnetic specific heat of $FeSc_2S_4$ due to overestimation of C_{lat}.

Finally, in Fig. 9(a), we show a Schottky-like contribution reflecting the lowest-lying electronic levels of the Fe^{2+} ions, where spin and orbital degrees of freedom are coupled giving rise to an entropy of $R\ln(10)$. The energy level scheme corresponds to the spin-orbital-singlet ground state, a first excited triplet, which was reported by THz spectroscopy and neutron diffraction [9,11], followed by a doublet, a triplet, and another singlet state. To calculate this electronic contribution, we used the expressions

$$C_{low-lying}(T) = N\frac{\partial E}{\partial T}, \qquad (1)$$

$$E = \frac{1}{Z}\sum_{i=0}^{5} g_i \epsilon_i e^{-\beta \epsilon_i}, \qquad (2)$$

and the partition function

$$Z = \sum_{i=0}^{5} g_i e^{-\beta \epsilon_i}, \tag{3}$$

with the excitation energies $\varepsilon_{0,1,2} = 0$, 2.5, 8, 11, 13 meV; the degeneracies $g_{0,1,2} = 1$, 3, 2, 3, 1, and $\beta \equiv 1/k_B T$. Note that only the energy of the first excited triplet has been observed by THz and neutron studies with energy of about 4.5 meV. By assuming a lower value of 2.5 meV, we parameterized the actual triplet dispersion as measured by neutron scattering [5] in a single-ion picture. The resulting curve is in good agreement with the residual specific heat for all samples and accounts well for the entropy at low temperatures.

Summarizing, we conclude that the total specific heat of all samples can be reasonably well explained by phononic contributions and the contribution from the low-lying electronic levels of Fe^{2+} ions, where spin and orbital degrees of freedom are entangled. No ordering phenomena are necessary to explain the experimental specific heat.

IV. CONCLUDING REMARKS

Our detailed structural, magnetic, and specific heat studies performed on polycrystalline and single crystalline samples of $FeSc_2S_4$ with well-controlled composition testify to the following important peculiarities of this material:

(1) The single-crystal x-ray diffraction demonstrated the presence of the pure spinel phase in the stoichiometric samples and revealed the second phase in the off-stoichiometric samples with Fe excess. The excess Fe forms a second phase with a regular diffraction pattern corresponding to a vacancy ordered iron sulfide with composition close to the 5C polytype of pyrrhotite (Fe_9S_{10}). The second phase is hardly detectable in the powder diffraction pattern of the off-stoichiometric samples.

(2) The structural analysis points to an extremely low level of inversion of the spinel phase in both stoichiometric and off-stoichiometric samples.

(3) The susceptibility of the stoichiometric samples ($x = 0$) follows a CW law in an extended temperature range from 10 to 400 K and does not reveal any sign of long-range magnetic order down to the lowest measured temperature of 1.8 K. No magnetic irreversibility is detected for these samples, indicating the absence of magnetic disorder.

(4) The susceptibility of the off-stoichiometric samples with Fe excess ($x > 0$) exhibits a significant field dependence at high temperatures, indicating additional magnetic contribution due to the second phase revealed by x-ray diffraction. It manifests pronounced magnetic irreversibility below 80 K with a clear splitting of ZFC and FC curves and the appearance of magnetic hysteretic effects. The second phase shows a transition into the paramagnetic state at temperatures above 580 K.

(5) The specific heat of the stoichiometric samples ($x = 0$) and the off-stoichiometric samples ($x > 0$) is dominated by the lattice contribution at temperatures above 50 K. Below 50 K, down to the lowest temperatures, no sharp anomaly in the specific heat characteristic of long-range magnetic or structural transformations is detected.

(6) Below 20 K, both stoichiometric and off-stoichiometric samples develop a similar broad feature in the specific heat which can be reasonably well explained by a contribution from the low-lying electronic levels of Fe^{2+} ions with entangled spin and orbital degrees of freedom of the main $FeSc_2S_4$ phase.

(7) Our results provide evidence for magnetic ordering in $FeSc_2S_4$ samples [14], which reflects the presence of excess iron in the respective samples. Stoichiometric $FeSc_2S_4$ does not exhibit magnetic order, as reported earlier, and is the prime candidate for a spin-orbital liquid.

[1] P. W. Anderson, Phys. Rev. **102**, 1008 (1956).

[2] L. Balents, Nature **464**, 199 (2010).

[3] L. Pawlak and M. Duczmal, Int. J. Modern Phys. **7**, 1020 (1993).

[4] V. Fritsch, J. Hemberger, N. Büttgen, E.-W. Scheidt, H.-A. Krug von Nidda, A. Loidl, and V. Tsurkan, Phys. Rev. Lett. **92**, 116401 (2004).

[5] A. Krimmel, M. Mücksch, V. Tsurkan, M. M. Koza, H. Mutka, and A. Loidl, Phys. Rev. Lett. **94**, 237402 (2005).

[6] G. M. Kalvius, O. Hartmann, D. R. Noakes, F. E. Wagner, R. Wäppling, U. Zimmermann, Ch. Baines, A. Krimmel, V. Tsurkan, and A. Loidl, Physica B **378–380**, 592 (2006).

[7] N. Büttgen, J. Hemberger, V. Fritsch, A. Krimmel, M. Mücksch, H.-A. Krug von Nidda, P. Lunkenheimer, R. Fichtl, V. Tsurkan, and A. Loidl, New J. Phys. **6**, 191 (2004).

[8] N. Büttgen, A. Zymara, C. Kegler, V. Tsurkan, and A. Loidl, Phys. Rev. B **73**, 132409 (2006).

[9] L. Mittelstädt, M. Schmidt, Z. Wang, F. Mayr, V. Tsurkan, P. Lunkenheimer, D. Ish, L. Balents, J. Deisenhofer, and A. Loidl, Phys. Rev. B **91**, 125112 (2015).

[10] N. J. Laurita, J. Deisenhofer, L.-D. Pan, C. M. Morris, M. Schmidt, M. Johnsson, V. Tsurkan, A. Loidl, and N. P. Armitage, Phys. Rev. Lett. **114**, 207201 (2015).

[11] A. Biffin, Ch. Ruegg, J. Embs, T. Guidi, D. Cheptiakov, A. Loidl, V. Tsurkan, and R. Coldea, Phys. Rev. Lett. **118**, 067205 (2017).

[12] G. Chen, L. Balents, and A. P. Schnyder, Phys. Rev. Lett. **102**, 096406 (2009).

[13] G. Chen, A. P. Schnyder, and L. Balents, Phys. Rev. B **80**, 224409 (2009).

[14] K. W. Plumb, J. R. Morey, J. A. Rodriguez-Rivera, H. Wu, A. A. Podlesnyak, T. M. McQueen, and C. L. Broholm, Phys. Rev. X **6**, 041055 (2016).

[15] J. R. Morey, K. W. Plumb, C. M. Pasco, B. A. Tramp, T. M. McQueen, and S. M. Koohpayeh, J. Crystal Growth **454**, 128 (2016).

[16] A. Tomas, M. Guittard, J. Rigoult, and B. Bachet, Mat. Res. Bul. **14**, 249 (1979).

[17] A. Tomas, M. Guittard, E. Barthelemy, and J. Flahaut, Mat. Res. Bul. **16**, 1213 (1981).

[18] See Supplemental Material at http://link.aps.org/supplemental/10.1103/PhysRevB.96.054417 for details of preparation and characterization of the crystals.

[19] CrysAlisPro, Agilent Technologies, Version 1.171.37.35 (release 13-08-2014 CrysAlis171 .NET) (compiled Aug 13, 2014,18:06:01).

[20] G. M. Sheldrick, Acta Cryst. C **71**, 3 (2015).

[21] J. Rodriguez-Carvajal, Physica B **192**, 55 (1993).

[22] A. V. Powell, P. Vaqueiro, K. S. Knight, L. C. Chapon, and R. D. Sánchez, Phys. Rev B **70**, 014415 (2004).

[23] H. Wang and I. Salveson, Phase Transitions **78**, 547 (2005).

[24] A. D. Elliot, Acta Cryst. B **66**, 271 (2010).

[25] F. K. Lotgering, Philips. Res. Rep. **11**, 190 (1956).

[26] S. A. Altschuler and B. M. Kozyrev, *Electron Paramagnetic resonance in Transition Element Compounds* (Nauka, Moscow, 1972), p. 428.

[27] J. A. Mydosh, *Spin Glasses: An Experimental Introduction* (Taylor and Francis, London, 1993).

[28] M. Charilaou, J. Kind, D. Koulialias, P. G. Weidler, C. Mensing, J. F. Löffler, and A. U. Gehring, J. Appl. Phys. **118**, 083903 (2015).

[29] D. Koulialias, J. Kind, M. Charilaou, P. G. Weidler, J. F. Löffler, and A. U. Gehring, Geophys. J. Int. **204**, 961 (2016).